Supplement of

Chemical properties, sources and size-resolved hygroscopicity of submicron black carbon-containing aerosols in urban Shanghai

Shijie Cui[1], Dan Dan Huang[2], Yangzhou Wu[1,a], Junfeng Wang[1], Fuzhen Shen[1,b], Jiukun Xian[1], Yunjiang Zhang[1], Hongli Wang[2], Cheng Huang[2], Hong Liao[1], Xinlei Ge[1,*]

[1] Jiangsu Key Laboratory of Atmospheric Environment Monitoring and Pollution Control, Collaborative Innovation Center of Atmospheric Environment and Equipment Technology, School of Environmental Science and Engineering, Nanjing University of Information Science and Technology, Nanjing 210044, China

[2] Shanghai Academy of Environmental Sciences, Shanghai 200233, China

[a]now at: Department of Atmospheric Sciences, School of Earth Sciences, Zhejiang University, Hangzhou 310027, PR China

[b]now at: Department of Meteorology, University of Reading, Reading, RG6 6BX, UK

*Corresponding author: Xinlei Ge (Email: caxinra@163.com)

For *Atmospheric Chemistry and Physics*

Table S1: Summary of the input parameters and uncertainties (±σ) for the calculations of hygroscopic parameters.

Parameter	average values	Uncertainty	Reference
O/C	0.26	±0.06	Measured from SP-AMS
κ_{AN}	0.58	±0.01	Gysel et al., (2007)
κ_{AS}	0.48	±0.01	Gysel et al., (2007)
κ_{AHS}	0.56	±0.01	Gysel et al., (2007)
κ_{OA} / (O / C)	0.29	±0.05	Chang et al.,(2010)
$\kappa_{\mathrm{rBC\text{-}rich}}$	0.09	±0.02	Chang et al.,(2010)
$\kappa_{\mathrm{HOA\text{-}rich}}$	0.02	±0.01	Chang et al.,(2010)
κ_{BBOA}	0.03	±0.01	Chang et al.,(2010)
$\kappa_{\mathrm{WS\text{-}HOA}}$	0.09	±0.02	Chang et al.,(2010)
$\kappa_{\mathrm{LO\text{-}OOA}}$	0.07	±0.01	Chang et al.,(2010)
$\kappa_{\mathrm{MO\text{-}OOA}}$	0.16	±0.03	Chang et al.,(2010)
$\kappa_{r\mathrm{BC}}$	0		
$\varepsilon_{\mathrm{AN}}$	0.192	±0.083	Wu et al., (2016)
$\varepsilon_{\mathrm{AS}}$	0.089	±0.064	Wu et al., (2016)
$\varepsilon_{\mathrm{AHS}}$	0.024	±0.016	Wu et al., (2016)
$\varepsilon_{\mathrm{rBC\text{-}rich}}$	0.089	±0.043	Wu et al., (2016)
$\varepsilon_{\mathrm{HOA\text{-}rich}}$	0.099	±0.065	Wu et al., (2016)
$\varepsilon_{\mathrm{BBOA}}$	0.044	±0.034	Wu et al., (2016)
$\varepsilon_{\mathrm{WS\text{-}HOA}}$	0.104	±0.083	Wu et al., (2016)
$\varepsilon_{\mathrm{LO\text{-}OOA}}$	0.071	±0.046	Wu et al., (2016)
$\varepsilon_{\mathrm{MO\text{-}OOA}}$	0.115	±0.066	Wu et al., (2016)
$\varepsilon_{r\mathrm{BC}}$	0.196	±0.069	Wu et al., (2016)

Table S2: Summary of correlation coefficients between different *r*BCc OA factors and NR-PM_1 OA factors with the ship emission tracer (V) during ship emission period (SEP) and non-ship emission period (Non-SEP)(see main text for details), respectively.

		*r*BCc OA								NR-PM_1 OA			
	r	*r*BC	HOA-rich	*r*BC-rich	BBOA	WS-HOA	LO-OOA_{rBC}	MO-OOA_{rBC}	HOA_{rBC}	HOA	COA	LO-$OOA_{NR\text{-}PM1}$	MOOOA $_{NR\text{-}PM1}$
SEP	V	0.69	0.69	0.28	0.55	0.72	0.22	-0.15	0.71	0.84	0.08	0.64	0.02
No-SEP	V	-0.01	0.25	0.01	-0.01	-0.04	-0.15	-0.62	0.06	0.19	0.20	-0.26	-0.77

Figure S1: Location of the sampling site (red five-pointed star) and its surroundings. The bottom right inset figure shows the International Container Companies and the ports, and the top right inset figure shows the site location in the scale of Yangtze River Delta (Modified from © Google Map/image credit).

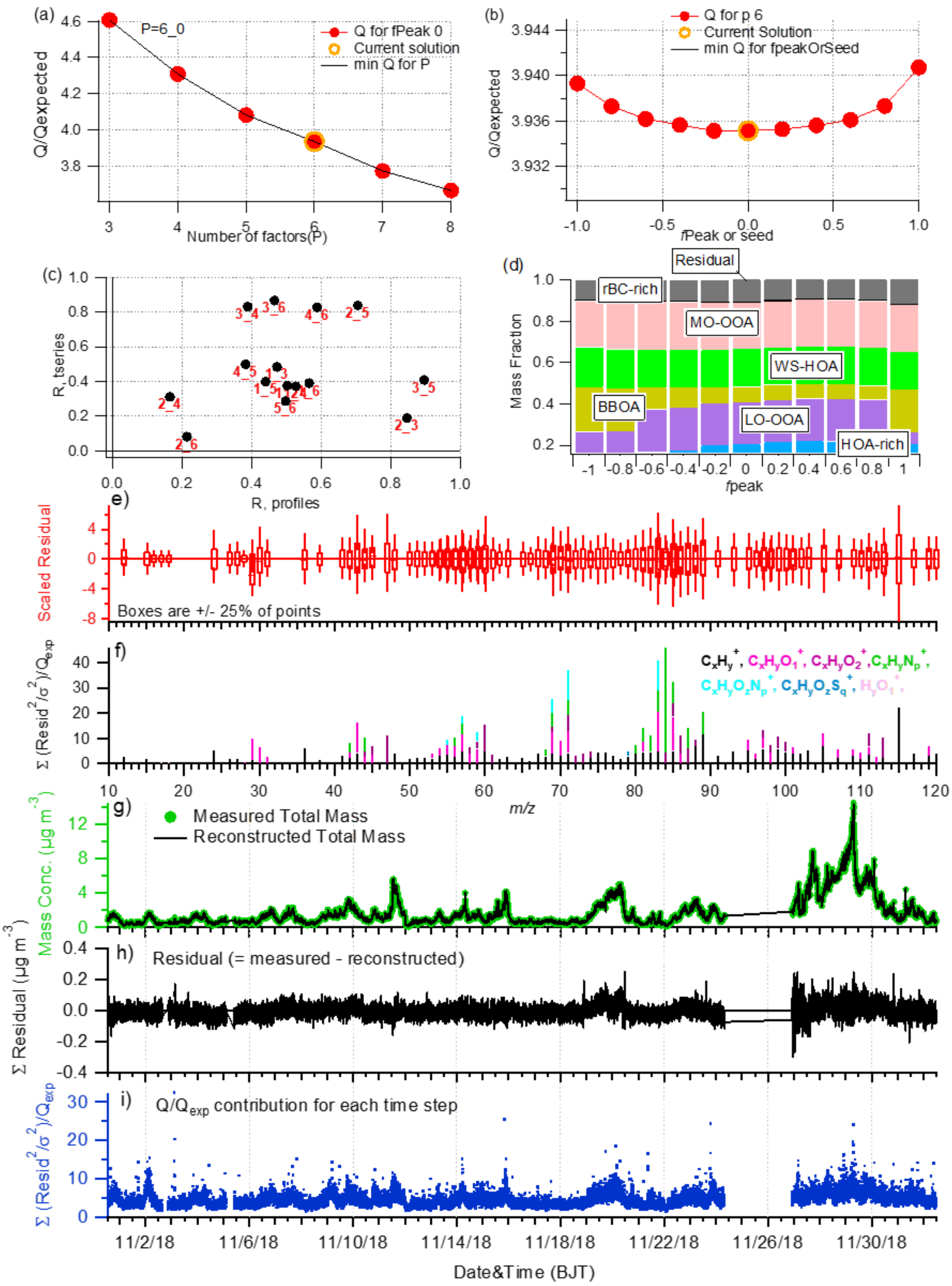

Figure S2. Summary of critical diagnostic plots of the PMF results for the 6-factor solution of *r*BCc OA: (a) Q/Q_{exp} as a function of the number of factors (P from 3 to 8). For the beat solution (6-factor): (b) Q/Q_{exp} as a function of *f*Peak, (c) cross-correlations of the time series and spectral profiles among the six factors, (d) fractions of OA factors as a function of *f*Peak, (e) the box and whiskers plot showing the distributions of scaled residuals for each *m/z*, (f) the Q/Q_{exp} values for each ion, (g) time series of the measured and the reconstructed OA mass loadings, (h) variations of the residuals of the fit, (i) the Q/Q_{exp} values for each time step.

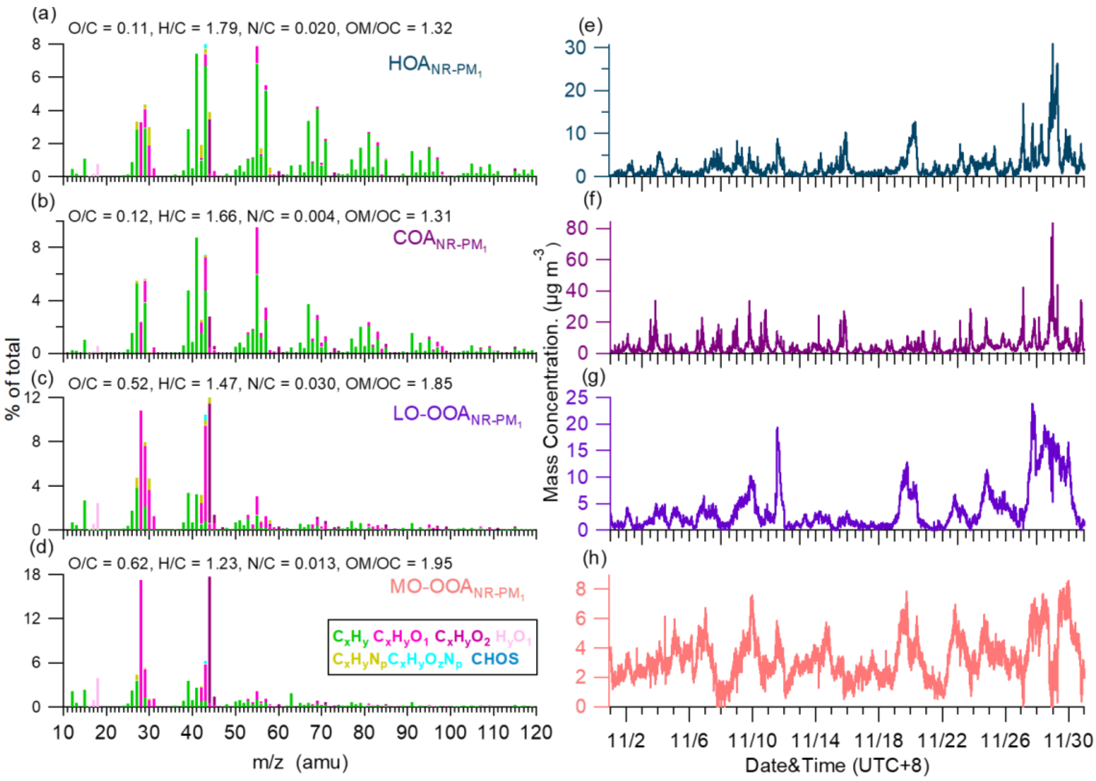

Figure S3. High resolution mass spectra (a-d) and time series (e-h) of the 4-factor solution resolved from PMF analysis of the NR-PM$_1$ OA.

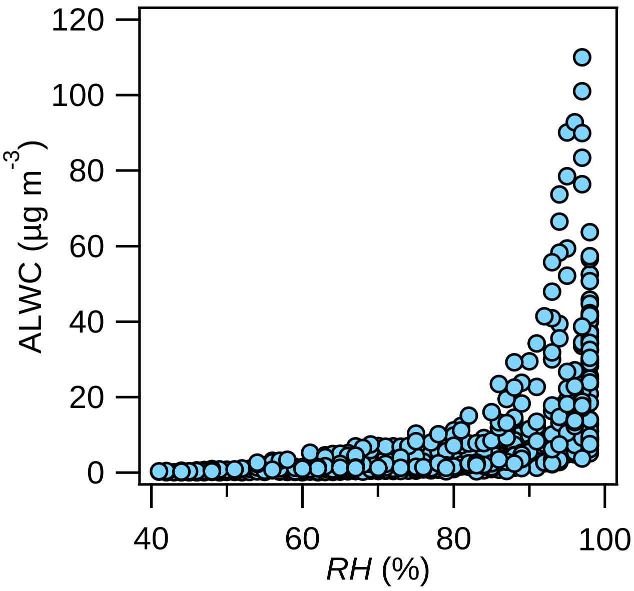

Figure S4. Calculated ALWC values versus RH for each time point (see main text for calculation details).

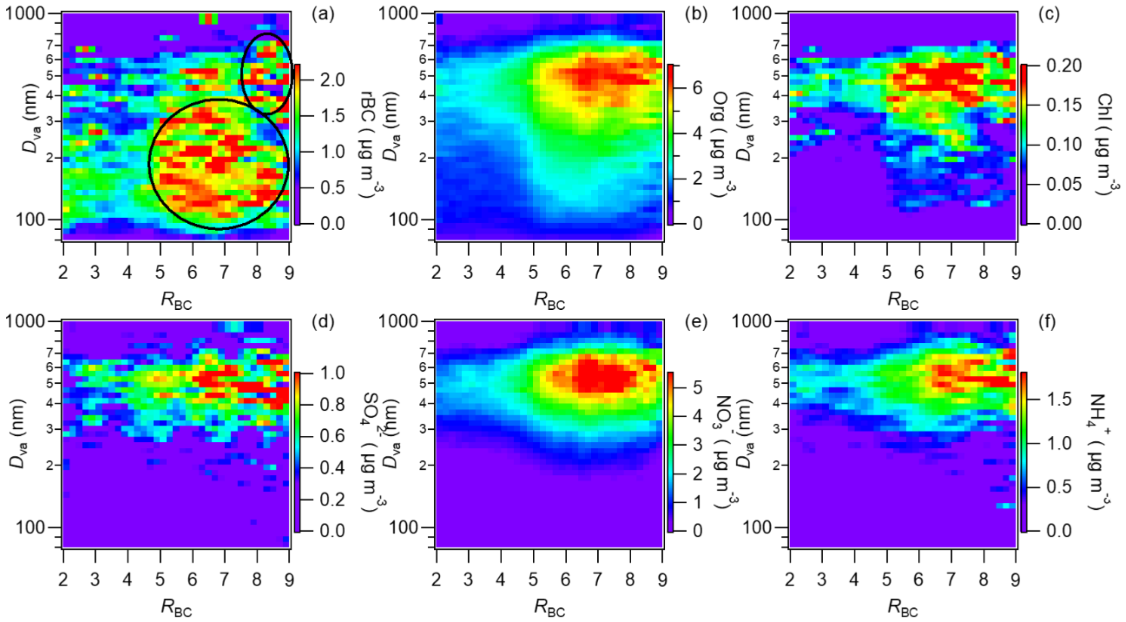

Figure S5. Image plots of size distributions of rBCc components as a function of R_{BC}.

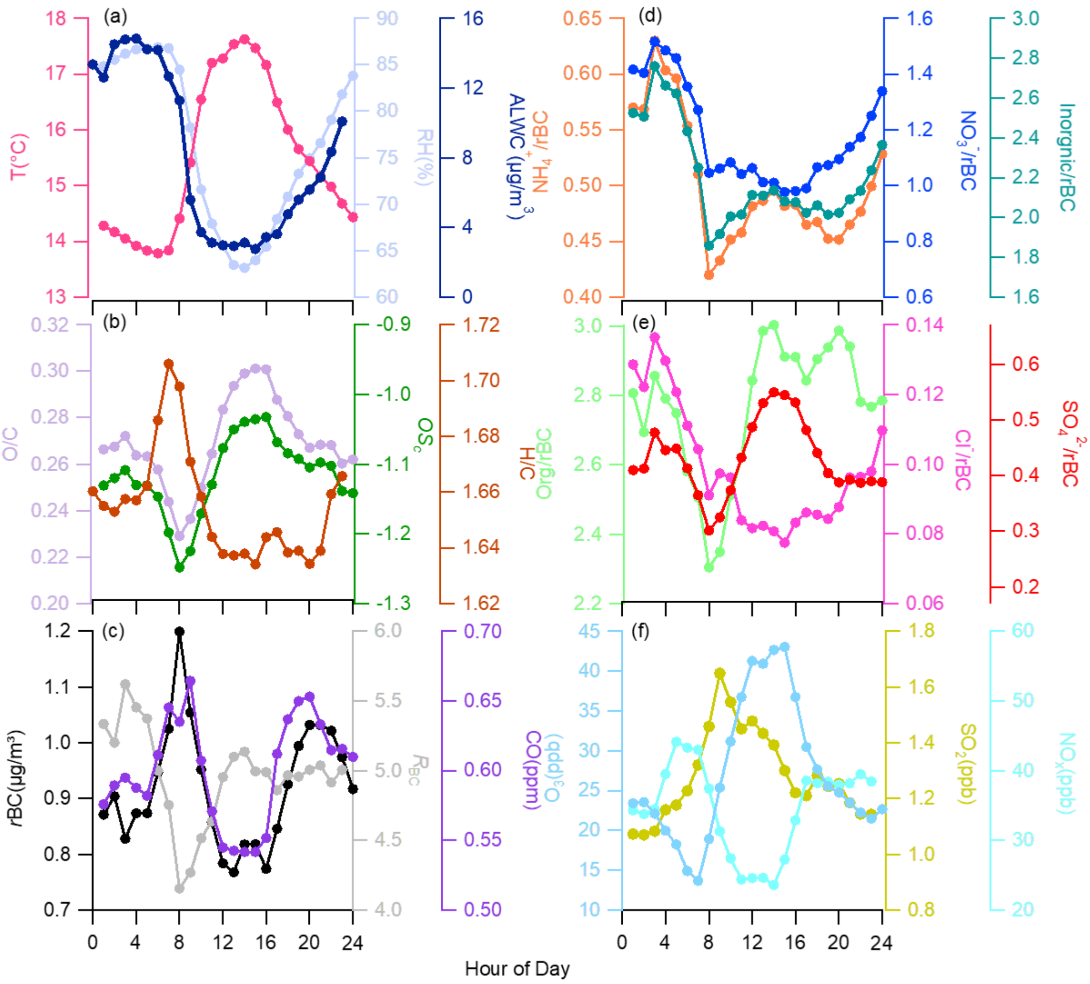

Figure S6. Campaign-average diurnal variations of (a) T, RH and ALWC, (b) O/C, H/C and oxidation state ($OS_C = 2\times O/C - H/C$), (c) R_{BC}, *r*BC and CO, (d) NO_3^-/*r*BC, NH_4^+/*r*BC and inorganics/*r*BC (inorganics=$NO_3^- + NH_4^+ + SO_4^{2-} + Cl^-$), (e) SO_4^{2-}/*r*BC, Cl^-/*r*BC and organics/*r*BC, and (f) gaseous species (O_3, SO_2, NO_X).

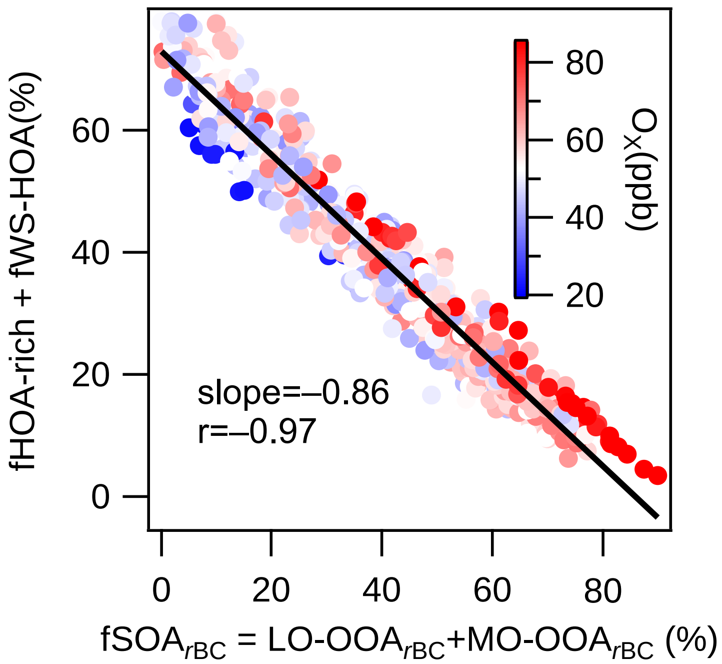

Figure S7. Relationship between the mass fraction (%) of the sum of HOA-rich and WS-HOA and the sum of LO-OOA$_{rBC}$ and MO-OOA$_{rBC}$) (colored by O_X concentrations).

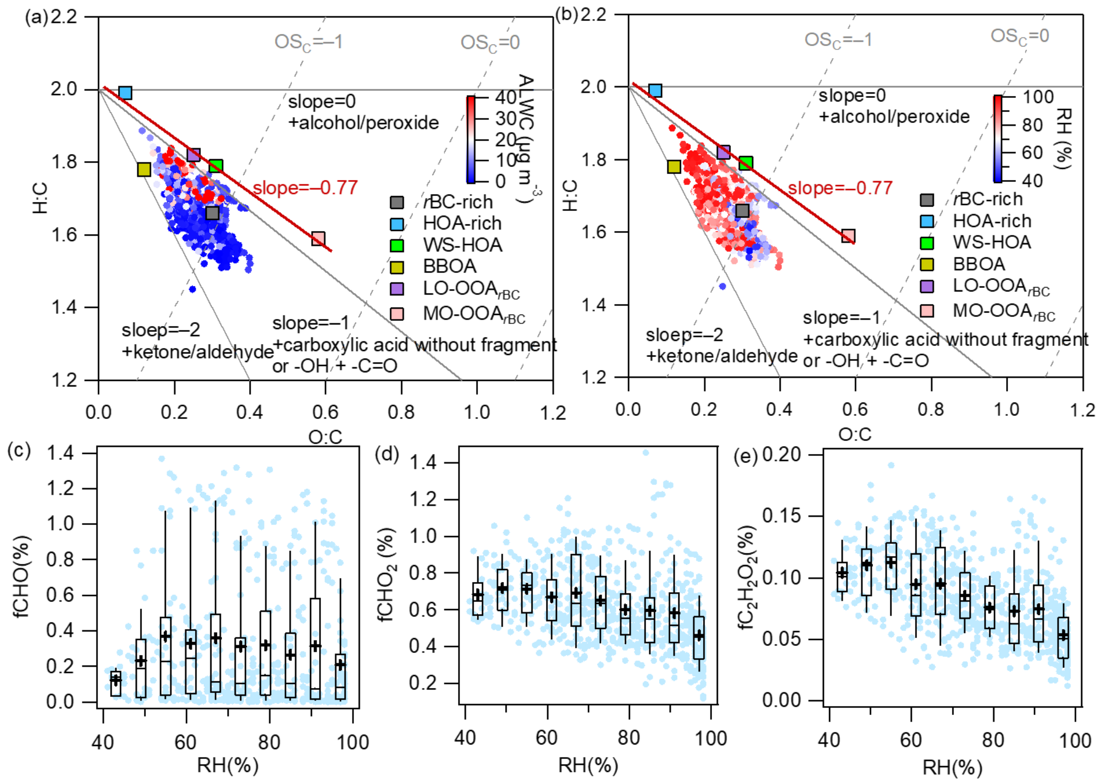

Figure S8. Van Krevelen diagram of H/C versus O/C ratios for all *r*BCc OA and the six factors colored by ALWC (a) and RH (b) (the red line is the fitted line of the four OA factors). (c-e) Mass fractions of selected oxygenated ion fragments as a function of RH (the whiskers above and below the boxes mark the 90% and 10% percentiles, respectively; the upper and lower edge of the boxes represent the 75% and 25% percentiles, respectively; and the lines and triangles inside the boxes denote the median and mean values, respectively).

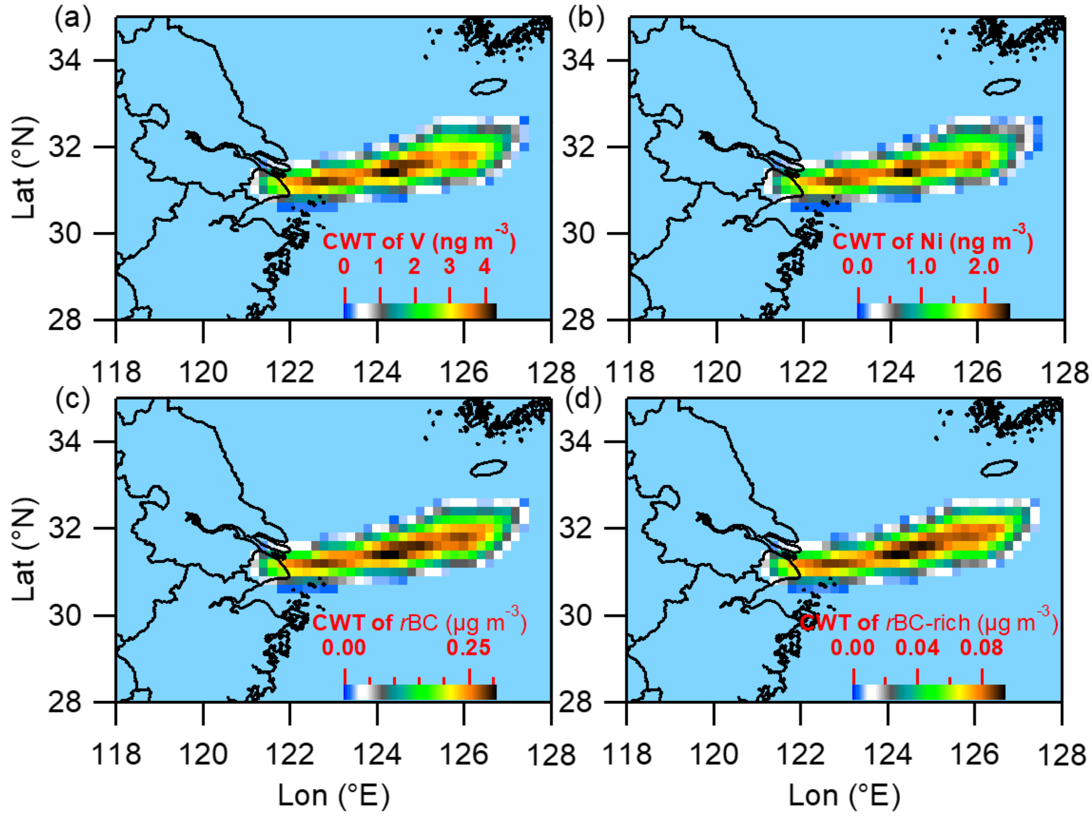

Figure S9. Concentration-weighted trajectories (CWT) of ship emission tracers of V (a) and Ni (b), and *r*BC (c) and *r*BC-rich OA factors (d) (the regions with high CWT values indicate potentially high concentrations of these species).

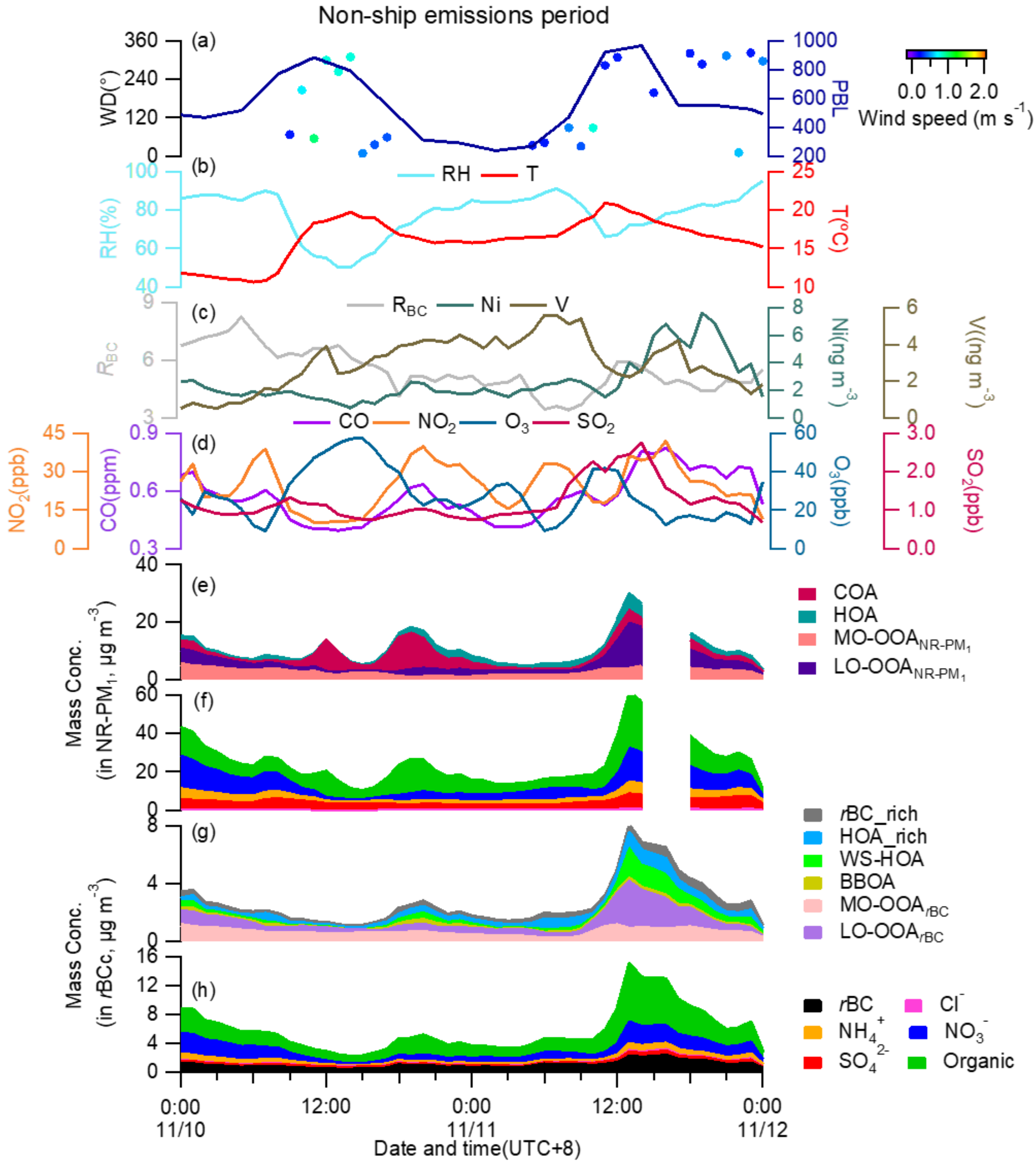

Figure S10. Time series of (a) wind direction (WD) colored by wind speed (WS), planetary boundary layer (PBL) height, (b) relative humidity (RH) and temperature (T), (c) mass concentrations of particle-phase Ni and V, and R_{BC}, (d) mass concentrations of CO, NO_2, O_3, SO_2, stacked concentrations of (e) NR-PM_1 OA factors, (f) NR-PM_1 species, (g) *r*BCc OA factors, and (h) *r*BCc components during the non-ship emission period (Non-SEP).

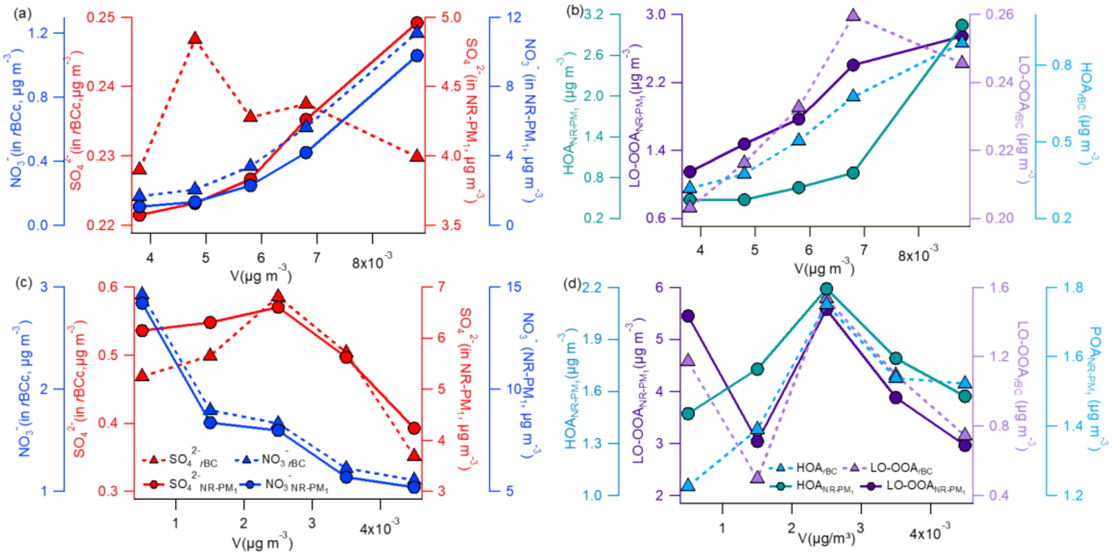

Figure S11. Mass concentrations of the *r*BCc nitrate, sulfate, OA factors in *r*BCc (dashed lines) and in NR-PM$_1$ (solid lines) as a function of V concentrations during ship emission period (a, b) and non-ship emission period (c, d).

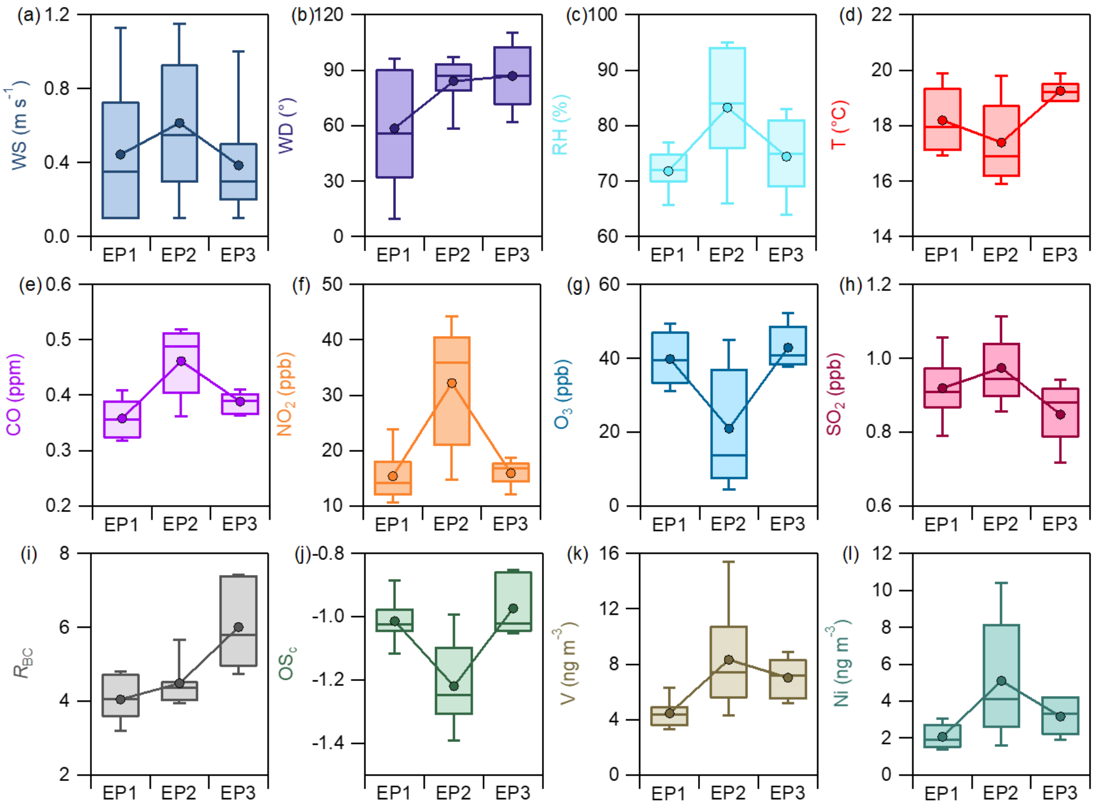

Figure S12. Box plots of meteorological parameters (a-d), gaseous pollutants (e-h), R_{BC} (i), OS_C (j), and ship emission tracers V (k) and Ni (l) of the three episodes during ship emission period (SEP)(meanings of the boxes are the same as those described in Fig. S8).

References

Chang, R. Y. W., Slowik, J. G., Shantz, N. C., Vlasenko, A., Liggio, J., Sjostedt, S. J., Leaitch, W. R., and Abbatt, J. P. D.: The hygroscopicity parameter (κ) of ambient organic aerosol at a field site subject to biogenic and anthropogenic influences: relationship to degree of aerosol oxidation, Atmos. Chem. Phys., 10, 5047-5064, https://doi.org/10.5194/acp-10-5047-2010, 2010.

Gysel, M., Crosier, J., Topping, D. O., Whitehead, J. D., Bower, K. N., Cubison, M. J., Williams, P. I., Flynn, M. J., McFiggans, G. B., and Coe, H.: Closure study between chemical composition and hygroscopic growth of aerosol particles during TORCH2, Atmos. Chem. Phys., 7, 6131-6144, https://doi.org/10.5194/acp-7-6131-2007, 2007.

Wu, Z. J., Zheng, J., Shang, D. J., Du, Z. F., Wu, Y. S., Zeng, L. M., Wiedensohler, A., and Hu, M.: Particle hygroscopicity and its link to chemical composition in the urban atmosphere of Beijing, China, during summertime, Atmos. Chem. Phys., 16, 1123-1138, https://doi.org/10.5194/acp-16-1123-2016, 2016.